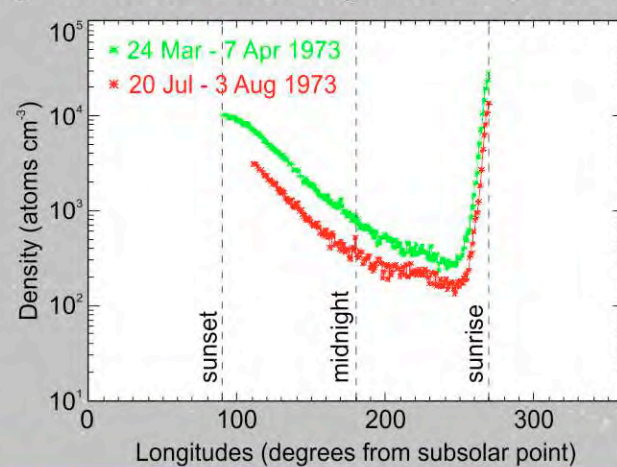


Argon as a Probe of Interior Out Gassing

- Argon, among the first elements to be discovered in the lunar exosphere, was seen only by the mass spectrometer LACE deployed during the Apollo 17 program [Hodges & Hoffman 1974];
- Argon-40, detected by LACE, comes from the interior of the Moon (by radioactive decay of Potassium-40).
- Its diurnal profile (Figure 1) showed peaks at terminators, and a decrease soon after sunset until the pre-dawn. The pre-dawn enhancement is explained by argon atoms coming from the hot dayside which overlap with freshly released argon atoms.
- Argon density was seen to decrease by a factor of 2 within 4 lunations, with small variations in smaller timescale.
- Subsequent attempts to detect argon have been unsuccessful until very recently [Cook et al., LPSC 2014, poster # 2788]
- Why its density decreased by a factor of 2? Is it just solar photo-ionization and charge-exchange with solar wind protons, or are there other sinks, such as cold-trapping in PSRs?
- Perhaps did LACE detect a local vent, or argon is released over large-scale fractures in the crust?

Figure 1: The maximum and minimum argon density measured by LACE over two different lunations, separated by 120 days. Digitized from Hodges [1975]. The data from the more recent lunation start slightly later, at ~110° longitude.



Lunar Exospheric Argon Modeling

- To answer these questions, a Monte Carlo simulation of lunar exospheric argon has been performed; longitude training trajectories of test particles.
- The particles are released uniformly across the lunar surface following a Maxwell-Boltzmann Flux distribution [Brinkmann, 1970].
- It follows the trajectory of test particles from the release until annihilation or cold-trapping.
- Once a particle impacts the regolith, it resides for a certain sticking (or residence) time, which depends on the surface temperature.

The Diviner Temperature Map Input

We used a global temperature map obtained by the Diviner instrument onboard LRO, generated by applying a model fit [Vasavada et al., 2012] to data from one orbit of LRO (Figure 2). We degraded such map to our coarser grid resolution (bins of 7.5° in longitude and 5° in latitude), and shifted in order to have noon at longitude 0° and midnight at longitude 180°.

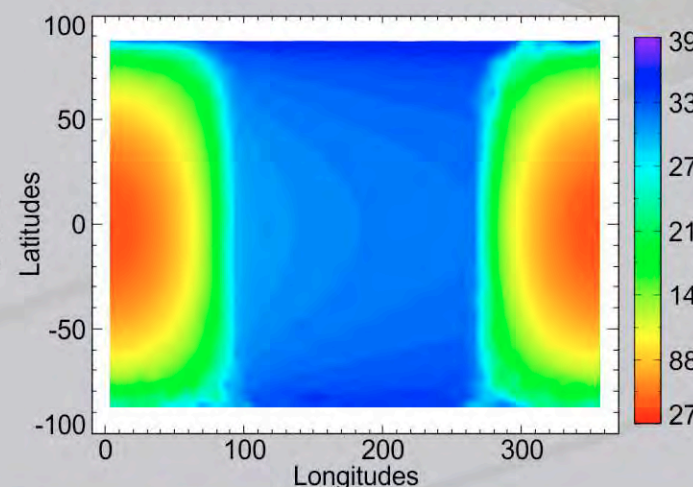


Figure 2: Diviner Temperature map expressed in K. The day of the map was October 8th, 2009, one day prior to the LCROSS impact.

The Residence Time

We take into account the residence time an argon atom spends adsorbed at the lunar surface:

$$t_{res} = \frac{C}{T} \exp\left(-\frac{4.19Q}{RT}\right) \quad [\text{Hodges, 1982}]$$

Q is the heat of adsorption (expressed in calories mole⁻¹), C is a constant (expressed in sec K²), 4.19 is the conversion between calories and Joules, and R is the gas constant.

Other works used different expressions for the residence time, which is highly uncertain even today (see Figure 3). We found agreement that the formulation of Hodges [1982] is the one that best describes the behavior of argon observed by LACE

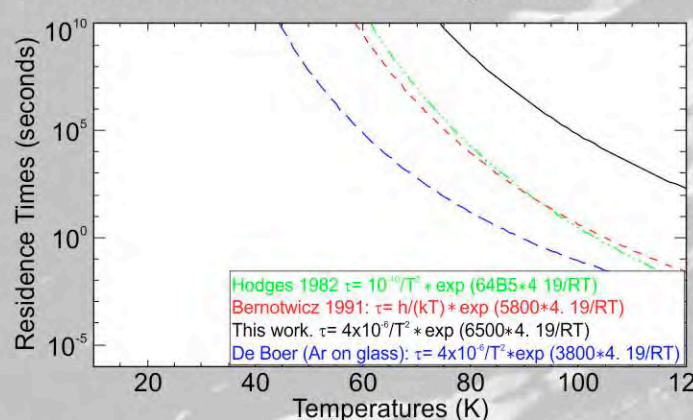


Figure 3: The desorption time (in seconds) for argon on different materials. The curve "de Boer" has been drawn using our formulation for the residence time with the value of Q derived for argon on glass [de Boer, 1968].

Global Argon Density in a Uniform Exosphere

Initially we aim to reproduce the characteristic nightside profile (the slope) of the density, and the relative intensities of sunrise and sunset peaks. We initialize the code with no losses so that the simulation reaches the steady state (Figure 4).

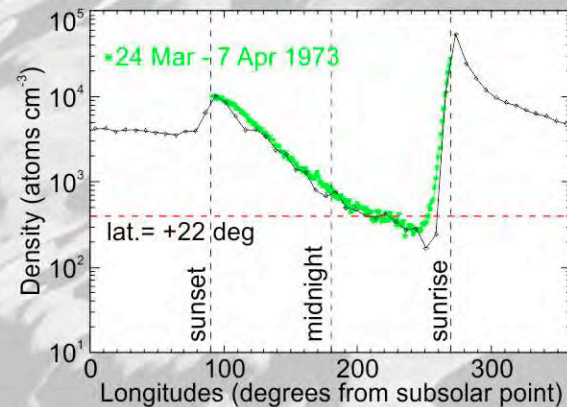


Figure 4: As Figure 1, including our steady-state simulation (black asterisk).

Global Argon Density in a Uniform Exosphere

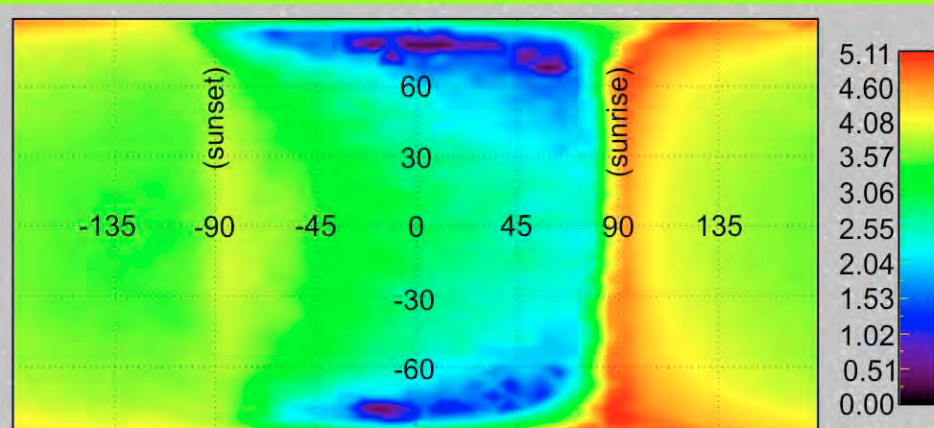


Figure 5: Global latitude-local time distribution of argon density (in logarithmic scale). The decrease of argon density during the night is shown from sunset at longitude -90° to sunrise at longitude +90°. A pre-sunrise increase appears.

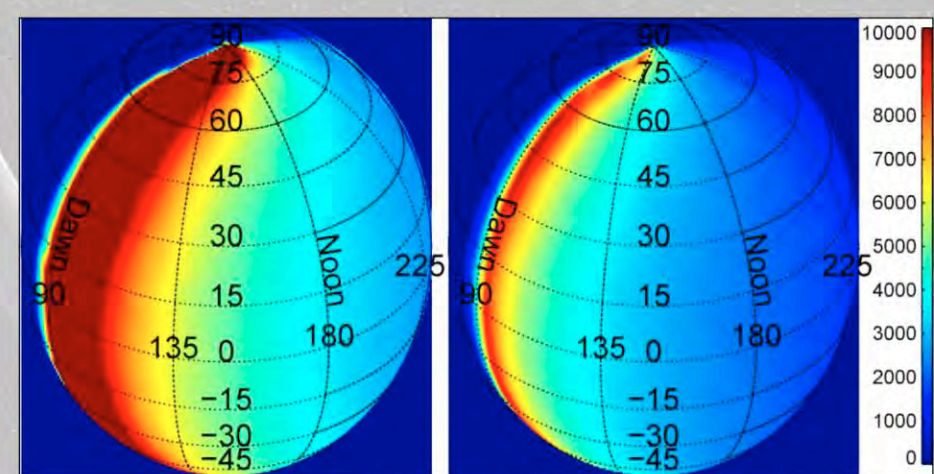


Figure 6: The argon density (in cm³) at 20 (left) and 45 (right) km altitude. The sub-observer longitude is at 30° longitude West of subsolar point, i.e. shortly before noon. Argon appears to be concentrated at the sunrise terminator (on the left in both globes).

Loss Processes

- Photo-ionization was determined to be the main source of loss for argon atoms in the lunar exosphere [Killen, 2002].
- Charge-exchange with solar wind protons has been generally neglected in previous studies, but we included it in our simulation to investigate its relative importance. We found that this latter process is, indeed, negligible.
- Solar Radiation Pressure is negligible and undetectable when introduced in our models (the difference is well below the statistical noise), due to the small g-factor of argon atoms for resonant scattering.

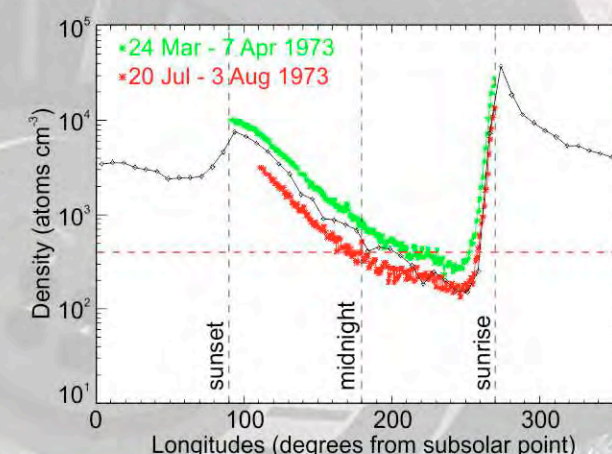


Figure 7: as Figure 1, including our model with solar photo-ionization and solar wind charge exchange (black asterisk). The density of argon doesn't reach the observed value after 120 days (red).

Cold Trapping in the Permanently Shaded Regions (PSRs)

That Permanently Shaded Regions (PSRs) could act as a reservoir for volatiles is an hypothesis proposed well before the advent of the Apollo program [Watson, 1961; Arnold, 1979].

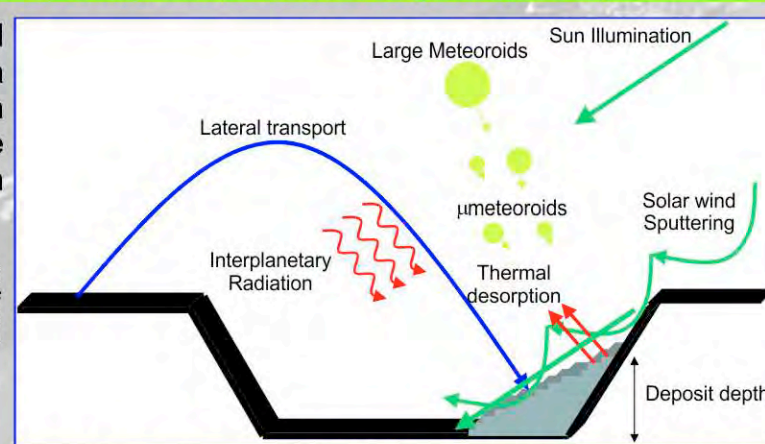


Figure 8: Schematic view of the main processes controlling the stability of argon deposits in permanently shaded regions.

We applied a stochastic approach that tracks the trapping in proximity of the polar region, using the most recent LRO/LOLA topography [Mazarico et al., 2011]. The PSR areas are 12,866 km² and 16,055 km² for the North and the South Pole, respectively, i.e. 1.99% and 2.48% of the area (6.6x10⁹ km²) of the cap within 15° from each pole (Figure 9). Using these values resulted in too much loss. Therefore, we reduced the value of the PSR at both poles by 10%.

Figure 10 illustrates how this amount of PSRs can account for the required additional loss process.

Figure 9: Permanently shadowed regions shown in color over a grayscale map of the average incident flux over four precession cycles. The smaller PSRs are displayed in cyan. From Mazarico et al., [2011]. We used 10% of these PSRs.

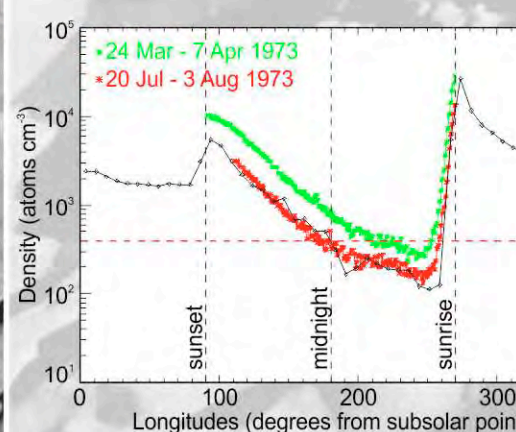
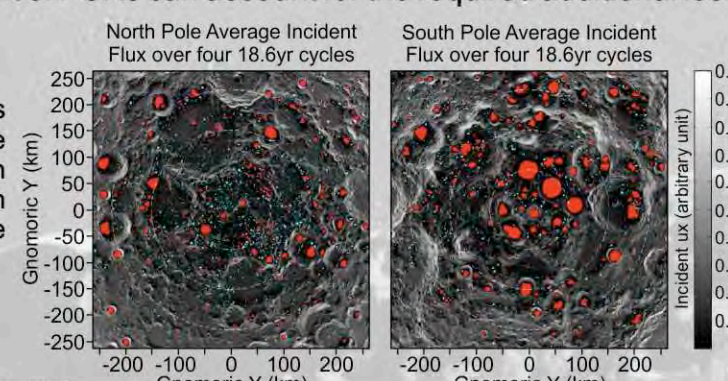


Figure 10: as Figure 7 including also cold-trapping on PSRs.

Moonquakes: Local or global release of argon?

- High Frequency Teleseismic (HFT) events [Nakamura et al., 1974] were invoked to explain the smaller density variations of argon seen by LACE.
- During the Apollo 17 measurements, seismometers of the Passive Seismic Experiment (PSE) recorded three such events just prior to each small-scale density enhancement.
- Binder [1980] estimated the amount of argon released during a moonquake. He found a range of 1.5x10²⁵–2.0x10²⁵ atoms of argon.
- Our initial estimate of argon population (1.4x10²⁶ argon atoms) is in agreement to these numbers.
- We performed another simulation releasing argon at one point on the surface, close to LACE, to test whether the release of argon occurred very close to LACE or not.
- In fact, HFT events are possibly correlated with impact basins [Nakamura et al., 1979], as well as deeper moonquakes, apparently generated along circular fault systems around impact basins [Runcom, 1974].
- Figure 11 shows that a global and a local venting of argon are indistinguishable after ~20 days from the release (less than 1 lunation).
- The plot of Figure 11 relative to day 6 shows that the density that LACE would have measured at sunrise is at least ~3 times the density at day 21, much higher than the actual measured increase in argon density. While a more rigorous simulation is needed, it seems likely that a localized release of argon can be ruled out.

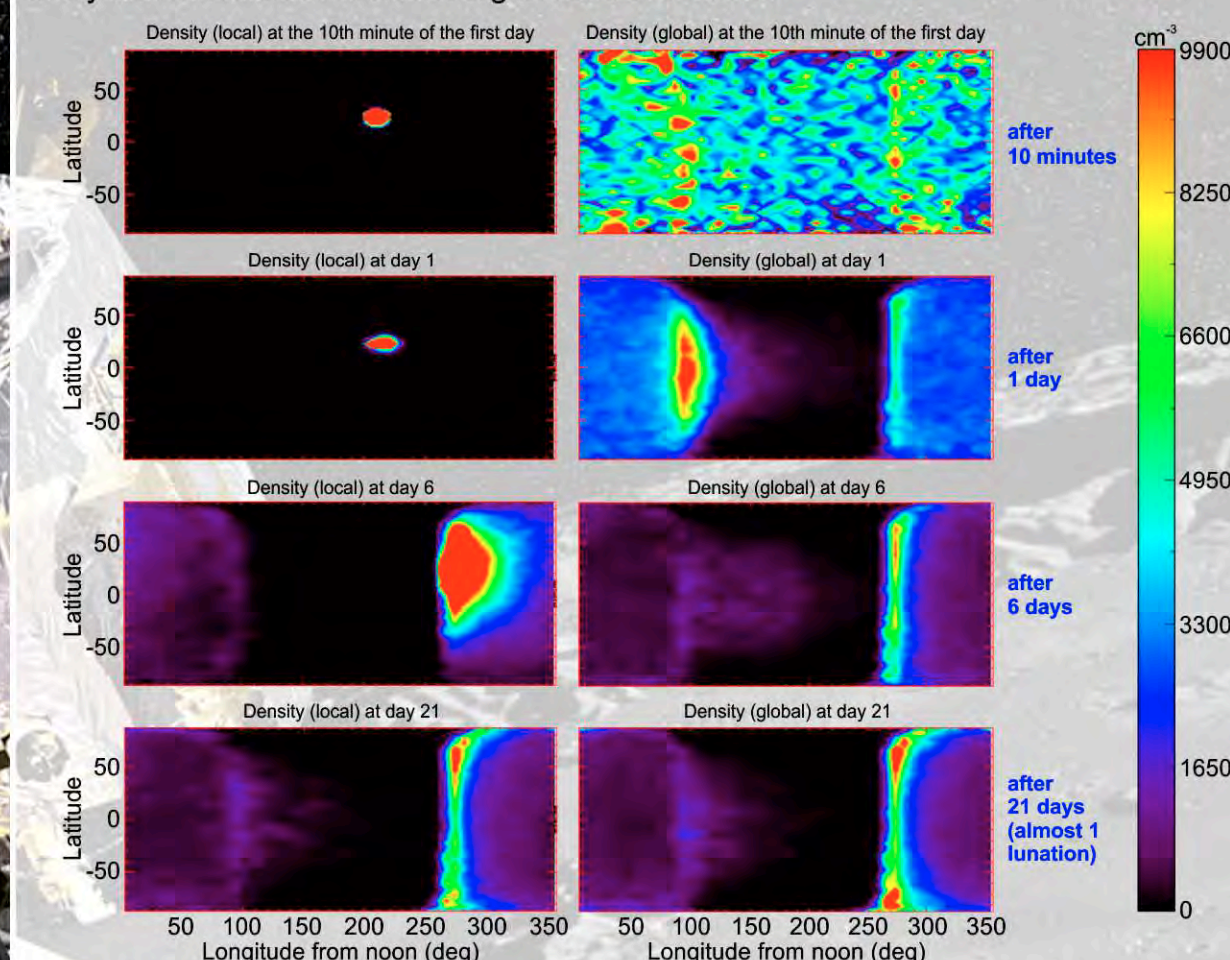


Figure 11: results of a simulation where argon was released locally (left) and globally (right). After 21 days, the local and the global release of argon resulted in nearly the same density. No losses were included here.

Adsorption of Argon on Water-contaminated Rocks

After 120 days of simulation, ~2000 kg of argon have been trapped. The required area of PSRs, 0.007% of the total lunar surface area correspond to a surface temperature of ~40 K. That is the temperature required for argon to adsorb, in the case of presence of water-contaminated surfaces [Hodges, 1980] (it's 70 K on dry rocks). Our results therefore suggest that water is adsorbed at least in the 10% of PSRs.

Normalized Histogram of Diviner Map

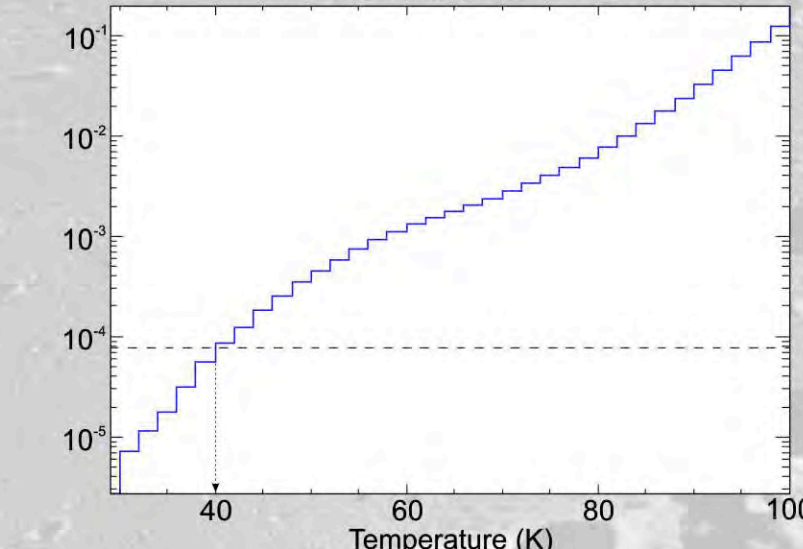


Figure 12: Cumulative distribution of points in the Diviner map lower than a certain temperature (x axis). Vertical axis has been normalized to 1. The horizontal dashed line corresponds to the total PSR area that we have introduced in our simulation, normalized to the total lunar surface.

The amount of adsorbed argon expected in Cabeus crater

An initial analysis of LAMP spectra of the LCROSS impact plume was performed by Gladstone et al. [2010], including a search for emission from the Ar-1048 Å resonant line. We report an upper limit brightness of ~1 Rayleigh, which, in the optically thin case, suggests a column density of 1.2x10¹³ cm⁻² (2-s upper limit) and a soil mass abundance of 5.8% (upper limit) in Cabeus crater, or 580 kg. This means that ~10⁸ such HFT events would need to have occurred since the time Cabeus became a PSR (>10⁷ years, Paige et al., 2010) assuming no subsequent loss or scavenging of trapped argon (the frequency of these HFT events averaged to 5 per year, according to Nakamura et al., 1979).

References

• Arnold, J. R. (1979). Ice in the lunar polar regions. *Journal of Geophysical Research: Solid Earth* (1978–2012), 84(B10), 5659–5668.
 • Bernotzowicz, T. J., & Podosek, F. A. (1981). Argon adsorption and the lunar atmosphere. In *Lunar and Planetary Science Conference Proceedings* (Vol. 21, pp. 307–313).
 • Binder, A. B. (1980). Shallow moonquakes: Argon release mechanism. *Geophysical Research Letters*, 7(11), 1011–1013.
 • Brinkmann, R. T. (1970). Departures from lunar escape rates for Ar and He in the Earth's atmosphere. *Planetary and Space Science*, 18(4), 449–476.
 • Cook, J. C.; Stern, S. A.; Feldman, P. D.; Retherford, K. D.; Gladstone, G. R.; Greathouse, T. K.; Grava, C.; Hurley, D. M.; Davis, M. W. (2014). Possible Detection of Argon in the Lunar Atmosphere as seen by the LAMP Instrument on the Lunar Reconnaissance Orbiter. *LPSC poster no. 2788*.
 • de Boer, J. H. (1968). The dynamical character of adsorption. *Soil Science*, 76(2), 156.
 • Gladstone, G. R.; Hurley, D. M.; Retherford, K. D.; Feldman, P. D.; Pryor, W. R.; Chaufray, J. Y.; Versteeg, M.; Greathouse, T. K.; Stern, S. A.; Bayless, A. J.; Cook, J. C.; Hurley, D. M.; Davis, M. W. (2010). LRO-LAMP observations of the LCROSS impact plume. *Science*, 330(6003), 472–476.
 • Hodges Jr., R. R. (1975). Formation of the lunar atmosphere. *The Moon*, 14(1), 139–157.
 • Hodges Jr., R. R. (1980). Lunar cold traps and their influence on argon-40. In *Lunar and Planetary Science Conference Proceedings* (Vol. 11, pp. 2463–2477).
 • Hodges, R. R. (1982). Adsorption of exospheric argon-40 in lunar regolith. In *Lunar and Planetary Science Conference Abstracts* (Vol. 13, pp. 329–330).
 • Hodges, R. R., and J.H. Hoffman (1974). Episodic release of Ar-40 from the interior of the moon. In *Lunar and Planetary Science Conference Proceedings*, 1974, p. 2955–2961.
 • Killen, R. M. (2002). Source and maintenance of the argon atmospheres of Mercury and the Moon. *Meteoritics & Planetary Science*, 37(9), 1223–1231.
 • Mazarico, E.; Neumann, G. A.; Smith, D. E.; Zuber, M. T.; & Torrence, M. H. (2011). Illumination conditions of the lunar polar regions using LRO topography. *Icarus*, 211(2), 1066–1081.
 • Nakamura, Y.; Dorman, J.; Duennebier, F.; Evans, M.; Lammlein, D.; Al-Lahyani, G. (1974). High-frequency lunar teleseismic events. In *Lunar and Planetary Science Conference Proceedings* (Vol. 5, pp. 2883–2890).
 • Nakamura, Y.; Latham, G. V.; Dorman, H. J.; Isahara, A. B.; Koyama, J.; & Horvath, P. (1979). Shallow moonquakes—Depth, distribution and implications as to the present state of the lunar interior. In *Lunar and Planetary Science Conference Proceedings* (Vol. 10, pp. 2299–2309).
 • Paige, D. A.; Siegler, M. A.; Zhang, J. A.; Hayne, P. O.; Foote, E. J.; Bennett, K. A.; Vasavada, A. R.; Greenhagen, B. T.; Schofield, J. T.; McCleave, D. J.; Foote, M. C.; DeJong, E.; Bills, B. G.; Harford, W.; Murray, B. C.; Allen, C. C.; Snook, K.; Soderblom, L. A.; Calcutt, B.; Taylor, F. W.; Bowles, N. E.; Bandfield, J. L.; Elphic, R.; Ghent, R.; Gloag, T. D.; Wynn, M. B.; and P. Lucy (2010). Diviner lunar radiometer observations of cold traps in the Moon's south polar region. *Science*, 330(6003), 479–482.
 • Runcom, S. R. (1974). On the origin of mascons and moonquakes. In *Lunar and Planetary Science Conference Proceedings* (Vol. 5, pp. 3115–3126).
 • Vasavada, A. R.; Bandfield, J. L.; Greenhagen, B. T.; Hayne, P. O.; Siegler, M. A.; Williams, J. F.; and D.A. Paige (2012). Lunar equatorial surface temperatures and regolith properties from the Diviner Lunar Radiometer Experiment. *Journal of Geophysical Research*, Volume 117, doi: 10.1029/2011JE003987.
 • Watson, K.; Murray, B. C.; & Brown, H. (1981). The behavior of volatiles on the lunar surface. *Journal of Geophysical Research*, 86(9), 3033–3045.